Journal of Magnetism and Magnetic Materials 575 (2023) 170747

Contents lists available at ScienceDirect

Journal of Magnetism and Magnetic Materials

journal homepage: www.elsevier.com/locate/jmmm

Hiemenz stagnation point flow with computational modelling of variety of boundary conditions

A.B. Vishalakshi [a], U.S. Mahabaleshwar [a,*], L.M. Pérez [b], O. Manca [c,*]

[a] Department of Studies in Mathematics, Shivagangotri, Davangere University, Davangere-577 007, India
[b] Departamento de Física, FACI, Universidad de Tarapacá, Casilla 7D, Arica, Chile
[c] Dipartimento di Ingegneria, Università degli Studi della Campania Luigi Vanvitelli, Aversa, CE, Italy

ARTICLE INFO

Keywords:
Unsteady case
Stagnation point flow
Nanofluid
Mass transpiration
Thermal radiation
Dual solutions

ABSTRACT

This work explains the flow of a *G-H_2O* nanofluid under the special case of MHD stagnation point flow, and the detailed investigation of the Navier's stokes equations extracted analytically. The main methodology is given work of PDEs is converted into ODEs using the appropriate similarity transformations. The momentum equations solved analytically to derive the solution domain, the impact of thermal radiation is seen in energy equation, four different scenarios are used to solve the energy equation. Aim of the present work is to study the theoretical analysis and it can be discussed for dual nature behavior by providing different physical parameters, these parameters control the domain, momentum and heat transpiration. In the heat transfer analysis solutions are derived in terms of incomplete gamma function and confluent hypergeometric form. The current work is examined using graphene nanoparticles, and the value of Pr is fixed at 6.2. The present problem is the benchmark solution for the results and it is significance in industrial and technological applications in fluid-based systems involving shrinkable/stretchable materials. At the end we get Velocity decreases with increases of V_C for upper branch of solution and increases with increases of V_C for lower branch of solution in the case shrinking sheet.

1. Introduction

Numerous researchers are interested in the problem of momentum and heat transfer due to its numerous industrial applications, including polymer extrusion, paper manufacturing, metal cooling, glass blowing, etc., [1]. Sakiadis [2,3] looks at stretching sheet issues initially. Crane [4] extended this issue with a 2-D flow resulting from a stretched sheet that was moving in its own plane at a variable speed. Numerous studies on the issues of stretching sheets have been conducted in part as a result of these works. In the presence of a magnetic field and radiation, Aly [5] studied the 2-D incompressible steady flow with metallic and non-metallic nanoparticles. Mahabaleshwar *et al.* [6] explained the theoretical investigation for unsteady flow due to impulsive stretching sheet problem. In the presence of a stretching sheet, Andersson et al. [7,8] investigated the magneto hydrodynamic flow of a power law and viscoelastic fluid. Mahabaleshwar *et al.* [9–12] examine the MHD effect for different types of fluid flow by using variety of boundary conditions with various physical parameters.

These experiments are restricted to the stretching sheet problems with different boundary conditions, further the investigations carried out with nanofluids. Most of all agree that nanofluid term is first introduced by Choi [13]. Nanofluids are the mixture of base fluids with nanoparticles. Nanoparticles are added to base fluids to obtain nanofluids. By using these nanofluids many investigations are carried out, Mahabaleshwar *et al.* [14] studied the nanofluid flow in the presence of magneto hydrodynamics with suction. In order to explain the thermal conductivity and viscosity of nanofluids, Sharifpur et al. [15,16] and Benos et al. [17] developed an asymptotic solution for nanofluid in a porous media that contained three different types of nanofluids: *Cu*, *Al_2O_3*, and *TiO_2*. See some other examples of nanofluids in [40–41]. One of the most beneficial nanomaterials is graphene, which combines two of the best qualities of materials: strength and thinness. For further information, check Reference [18]. Different physical properties and applications of graphene are clearly detailed in the references [19–20]. It is a better thermal and electrical conductor and optically transparent material when compared to other materials The exact solutions of graphene water nanofluid flow across a stretching/shrinking sheet in the presence of suction/injection heat source/sink in the presence of dual nature were also examined by Aly [21]. Additionally, take a look at Singh et al [22].

* Corresponding authors.
E-mail addresses: vishalavishu691@gmail.com (A.B. Vishalakshi), u.s.m@davangereuniversity.ac.in (U.S. Mahabaleshwar), lperez@academicos.uta.cl (L.M. Pérez), oronzio.manca@unicampania.it (O. Manca).

https://doi.org/10.1016/j.jmmm.2023.170747
Received 30 December 2022; Received in revised form 9 April 2023; Accepted 14 April 2023
Available online 20 April 2023

Nomenclature

b	Constants $(-)$
$B(x,t)$	Magnetic field strength $(Tesla)$
C_P	Specific heat at constant pressure $(Jkg^{-1}K^{-1})$
G	Graphene $(-)$
k^*	Mean absorption coefficient $(-)$
M	Kummer's function $(-)$
P	pressure (Nm^{-2})
q_r	Radiative heat flux $(-)$
q_w	Local heat flux (Wm^{-2})
R	Radiation parameter $(-)$
V_C	Mass transpiration $(-)$
T	Temperature (K)
(u,v)	Components of velocities (ms^{-1})
(x,y)	Coordinates (m)
V_w	Mass transfer velocity (ms^{-1})

Greek symbols

α	Wall moving parameter $(-)$
β	Solution domain $(-)$
ν	Kinematic viscosity (m^2s^{-1})
μ	Dynamic viscosity $(kgm^{-1}s^{-1})$
κ	Thermal conductivity (W/mK)
ξ	A variable $(-)$
σ	Electrical conductivity (Sm^{-1})
σ^*	Stefan Boltzmann constant $(Wm^{-2}K^{-4})$
ρ	Density (kgm^{-3})

Subscripts

w	Condition at wall $(-)$
∞	Condition at free stream $(-)$
η	Differentiation with respect to η $(-)$

Abbreviations

MHD	Magneto hydrodynamics $(-)$
PST	Prescribed surface temperature $(-)$
PHF	Prescribed heat flux $(-)$

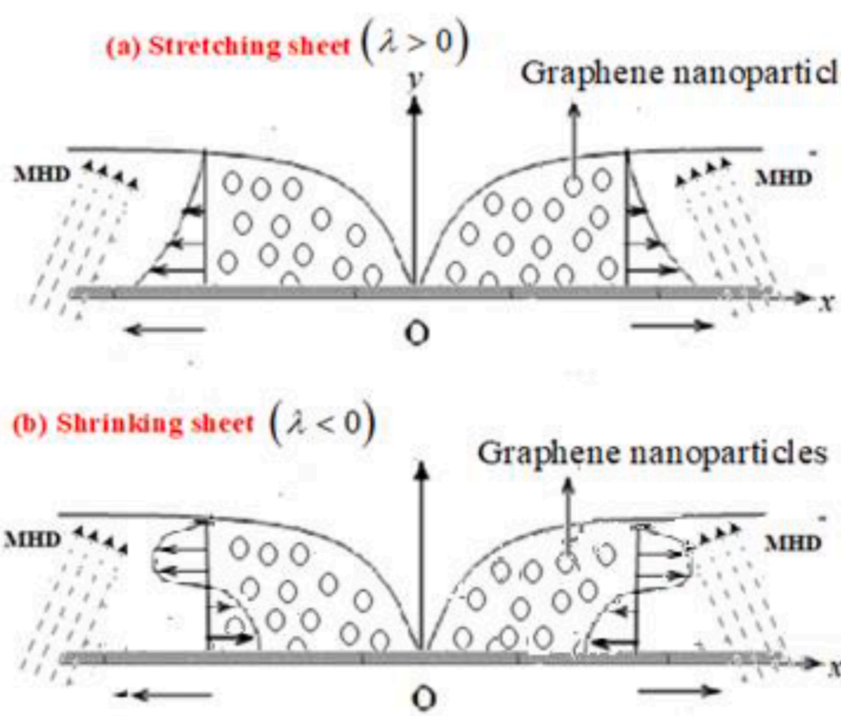

Fig. 1. Schematic diagram of fluid flow.

Based on the aforementioned research, the current work provides an explanation for the unsteady stagnation point flow caused by MHD sheet stretching and contracting along with thermal radiation and mass transpiration. Graphene nanoparticles are used to analyse the present analysis. The main methodology used in the current analysis is the energy equations are also solved under four different cases and represented in terms of incomplete gamma function as well as Kummer's function to provide the solution domain for the resultant ODEs. Analysing the results of the present can be done by employing different regulating parameters. The flow's dual nature can also be verified. It is possible to draw conclusions from the results using graphical representations. Fang et al. are effectively argued in the current study [23]. The scientific contribution of the present work is used in the field of crystal growing, continuous cooling, glass fibre production and entropy generation Also, the significance of nanoparticles with the fluid flow enhanced the convective heat transfer and lowered the friction characteristics, also higher flow rates the heat transfer characteristics and friction decreases.

2. Physical model and solution

In order to achieve the current analysis, we are considering the following assumptions it helps to understand the effect on fluid flow.

Table 1
Base fluid and nanoparticle thermophysical characteristics (See [30–31]).

	$C_P(J/kgK)$	$\rho(kg/m^3)$	$k(W/mK)$	$\sigma(\Omega/m)^{-1}$	Pr
Pure water (H_2O)	4179	997.1	0.613	0.05	6.2
Graphene(G)	2100	2250	2500	1×10^7	

- A laminar MHD two-dimensional unsteady stagnation point flow with a free stream velocity $U_\infty = bxt^{-1}$ is considered in the present analysis, here b is constant.
- $B(x,t)$ denotes the strength of magnetic field applied perpendicular to the surface and it is defined by $B(x,t) = B_0/t$.
- The physical scenario is schematically represented at Fig. 1. The x-axis moves away towards the free stream direction, and the y-axis runs perpendicular to it.
- Physical quantities of these nanofluids are represented at Table 1.
- $U_W = \frac{\alpha bx}{t}$ is x-direction velocity. The temperature at the wall is kept constant at T_w or with heat flux $\frac{q_w}{\sqrt{t}}$. T_∞ is the constant temperature of the free stream fluid.
- The governing 2-D Navier's stokes equation is given by (See Mahabaleshwar et al. [23], Anusha et.al.[24], Bhatti et al. [32], Hassan et al. [33]).

$$\frac{\partial u}{\partial x}+\frac{\partial v}{\partial y}=0 \tag{1}$$

$$\rho_{nf}\left(\frac{\partial u}{\partial t}+u\frac{\partial u}{\partial x}+v\frac{\partial u}{\partial y}\right) = -\frac{\partial P}{\partial x}+\mu_{nf}\left(\frac{\partial^2 u}{\partial x^2}+\frac{\partial^2 u}{\partial y^2}\right)+\sigma_{nf}B^2(x,t)(U_\infty-u) \tag{2}$$

$$\rho_{nf}\left(\frac{\partial v}{\partial t}+u\frac{\partial v}{\partial x}+v\frac{\partial v}{\partial y}\right) = -\frac{\partial P}{\partial y}+\mu_{nf}\left(\frac{\partial^2 v}{\partial x^2}+\frac{\partial^2 v}{\partial y^2}\right) \tag{3}$$

$$(\rho C_P)_{nf}\left(\frac{\partial T}{\partial t}+u\frac{\partial T}{\partial x}+v\frac{\partial T}{\partial y}\right)=\kappa_{nf}\left(\frac{\partial^2 T}{\partial x^2}+\frac{\partial^2 T}{\partial y^2}\right)-\frac{\partial q_r}{\partial y} \tag{4}$$

the suitable boundary conditions as

$$\left.\begin{aligned} u(x,0,t)&=\frac{\alpha bx}{t},\\ v(x,0,t)&=V_w(x,t),\\ u(x,\infty,t)&=\frac{bx}{t}\end{aligned}\right\} \tag{5}$$

$$\left.\begin{aligned} &T=T_w,\quad T\to T_\infty \quad \text{for PST case}\\ &-\kappa\frac{\partial T}{\partial y}=\frac{q_w}{\sqrt{t}},\quad T\to T_\infty\quad \text{for PHF case}\end{aligned}\right\} \tag{6}$$

The Nomenclature contains definitions of the terms used in Eqs. (1) to (6).

Similarity variables can be defined as

$$\psi(x,y,t)=bf(\eta)x\sqrt{\frac{\nu}{t}}\eta=\frac{y}{\sqrt{\nu t}},\theta(\eta)=\frac{T-T_\infty}{T_w-T_\infty} \tag{7}$$

These are the components of velocity that can be defined using the stream function:

$$u=\frac{bx}{t}f_\eta(\eta),\quad v=-b\sqrt{\frac{\nu}{t}}f(\eta) \tag{8}$$

The velocity of wall transpiration is also provided by

$$V_w(x,t)=V_w(t)=-b\sqrt{\frac{\nu}{t}}f(0) \tag{9}$$

3. Solution of pressure term

The term $\frac{\partial P}{\partial y}$ is the function of t and y it can be calculated by Eq.(3), it means $\frac{\partial P}{\partial y} = \Phi(t,y)$, the integration of this derivative yields to get the following result

$$P=\int\phi(t,y)+\psi(t,x) \tag{10}$$

here, $\psi(t,x)$ is constant of integration.

Again differentiate Eq. (10) to get the equation as $\frac{\partial P}{\partial x}=\frac{\partial\psi(t,x)}{\partial x}$, this is free from y. then applying x-momentum with $u=U_\infty$, $\frac{\partial P}{\partial x}$ can be derived as

$$-\frac{1}{\rho_{nf}}\frac{\partial P}{\partial x}=\frac{\partial U_\infty}{\partial t}+U_\infty\frac{\partial U_\infty}{\partial x}=-\frac{bx}{t^2}+\frac{b^2x}{t^2} \tag{11}$$

The pressure gradient in the y-direction is similarly provided by

$$-\frac{1}{\rho_{nf}}\frac{\partial P}{\partial y}=\frac{\partial v}{\partial t}+v\frac{\partial v}{\partial y}-\nu_{nf}\frac{\partial^2 v}{\partial y^2} \tag{12}$$

The pressure can be derived from integrating Eq. (11) and (12), then the equation becomes

$$\frac{1}{\rho_{nf}}(P_0-P)=-\frac{bx^2}{2t^2}+\frac{b^2x^2}{2t^2}+\frac{b\nu}{2t}f(\eta)\eta+\frac{b^2\nu_f}{2t}f_\eta(\eta)+\frac{b\nu_{nf}}{t}f_\eta(\eta) \tag{13}$$

where, P_0 is constant obtained from the integration.

4. Exact solution for velocity

The following can be obtained by applying the similarity variables defined at Eqs. (7) and (8) in Eq. ODE

$$\frac{\varepsilon_1}{\varepsilon_2}f_{\eta\eta\eta}+\left(bf+\frac{\eta}{2}\right)f_{\eta\eta}+(1-bf_\eta)f_\eta+(b-1)+\frac{\varepsilon_3}{\varepsilon_2}bQ(1-f_\eta)=0 \tag{14a}$$

The boundary condition associated with this equation also reduced as

$$f_\eta(0)=\alpha,\quad f(0)=V_C,\quad f_\eta(\infty)=1 \tag{14b}$$

Here, $\alpha=\frac{U_w}{U_\infty}$ is the wall stretching parameter, $Q=\frac{\sigma_f B_0^2}{\rho_f bt}$ is the Chandrasekhar's number, $V_C=-\frac{V_w(x,t)}{b\sqrt{\nu/t}}$ represents mass transpiration, and the values of b determine mass transpiration.

We now explore a unique case considering $b = -1/2$, in Eq.(14a), then we yield

$$\frac{\varepsilon_1}{\varepsilon_2}f_{\eta\eta\eta}+\left(-\frac{1}{2}f+\frac{\eta}{2}\right)f_{\eta\eta}+\left(1+\frac{1}{2}f_\eta\right)f_\eta+\left(-\frac{1}{2}-1\right)+\frac{\varepsilon_3}{\varepsilon_2}\left(-\frac{1}{2}\right)Q(1-f_\eta)=0 \tag{15}$$

Defining a new transformation $F(\eta) = f(\eta)-\eta$, substituting this transformation in Eq. (15), then it becomes

$$\varepsilon_1F_{\eta\eta\eta}-\frac{\varepsilon_2}{2}FF_{\eta\eta}+2\varepsilon_2F_\eta+\frac{\varepsilon_2}{2}F_\eta^2-\frac{\varepsilon_3}{2}QF_\eta=0 \tag{16}$$

Eq. (14) of the corresponding boundary conditions also reduces to

$$F(0)=V_C,\quad F_\eta(0)=\alpha-1,\quad F_\eta(\infty)=0 \tag{17}$$

Assume Eq. (16) has a solution that takes the form

$$F(\eta)=c+dExp(-\beta\eta) \tag{18}$$

By using Boundary conditions defined at Eq. (17) the following results can be found

$$d=\frac{1-\alpha}{\beta},\quad c=V_C+\frac{1-\alpha}{\beta} \tag{19}$$

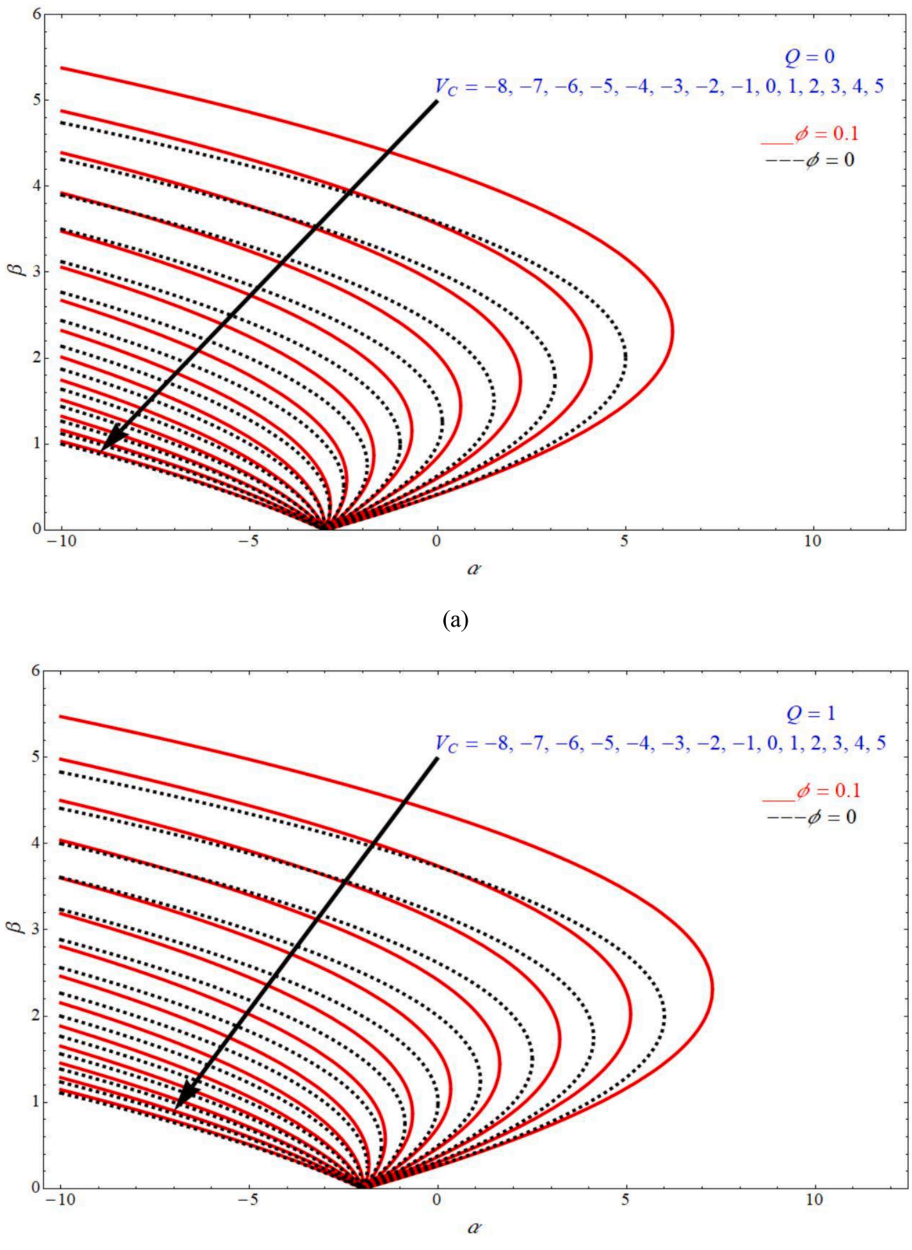

Fig. 2. β verses α for different V_C values.

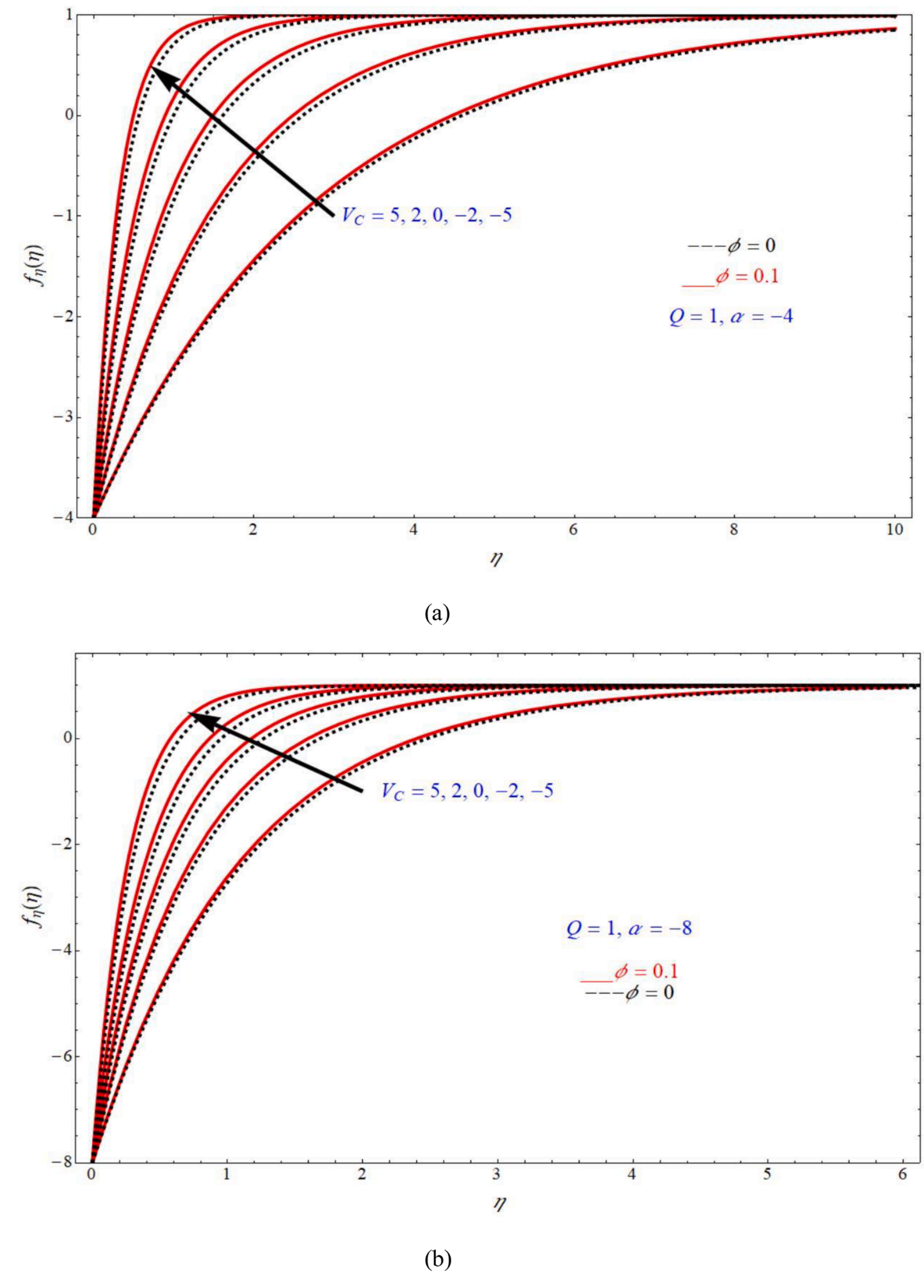

Fig. 3. $f_\eta(\eta)$ verses η for various V_C values at different α.

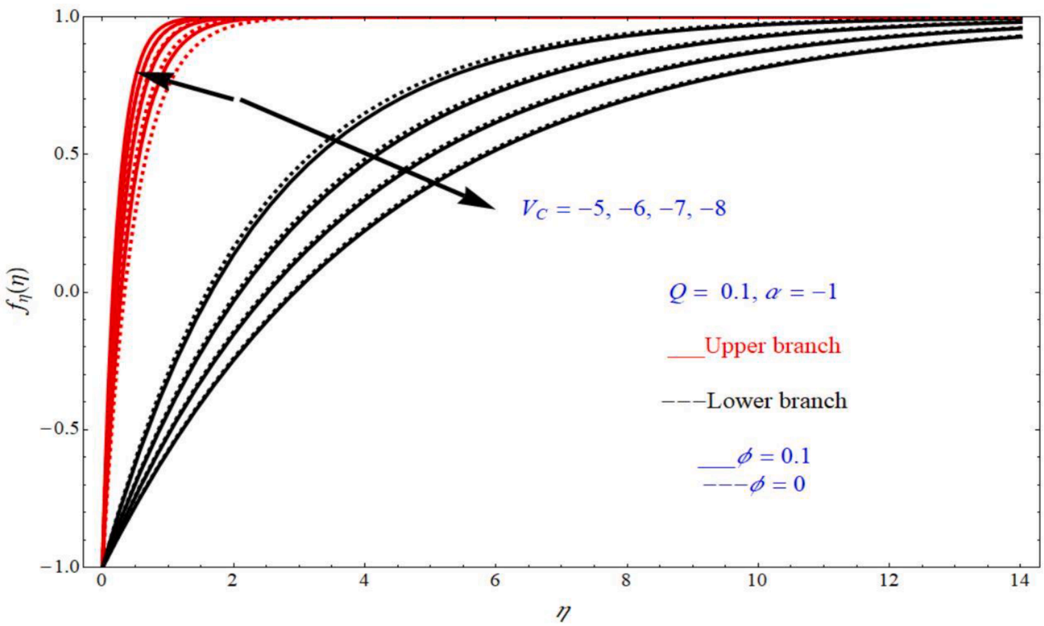

(a)

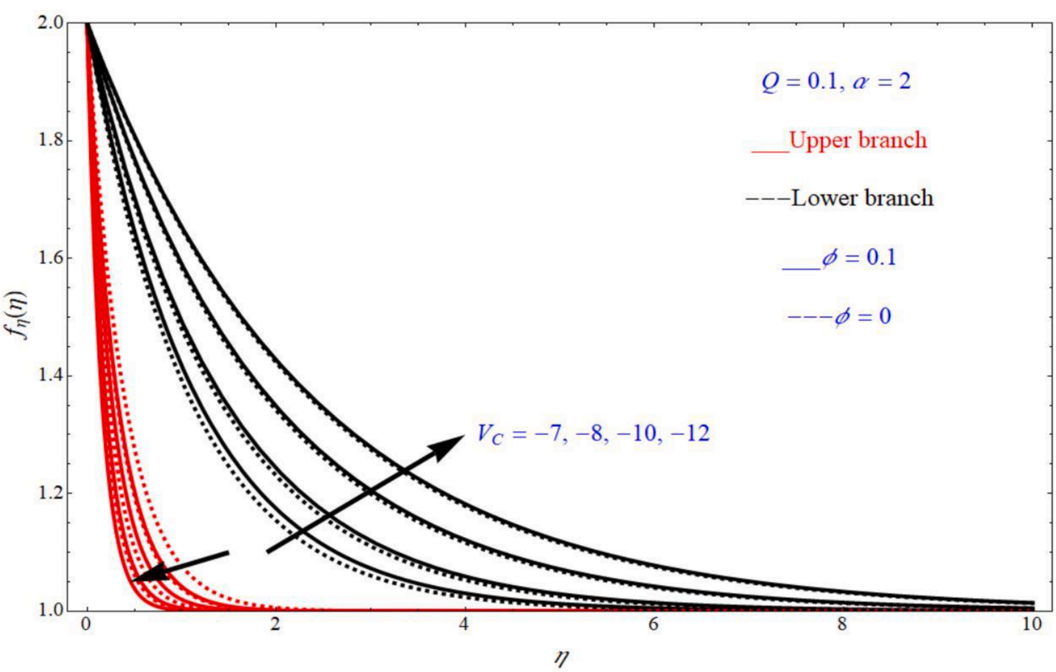

(b)

Fig. 4. $f_\eta(\eta)$ verses η for different choices of V_C.

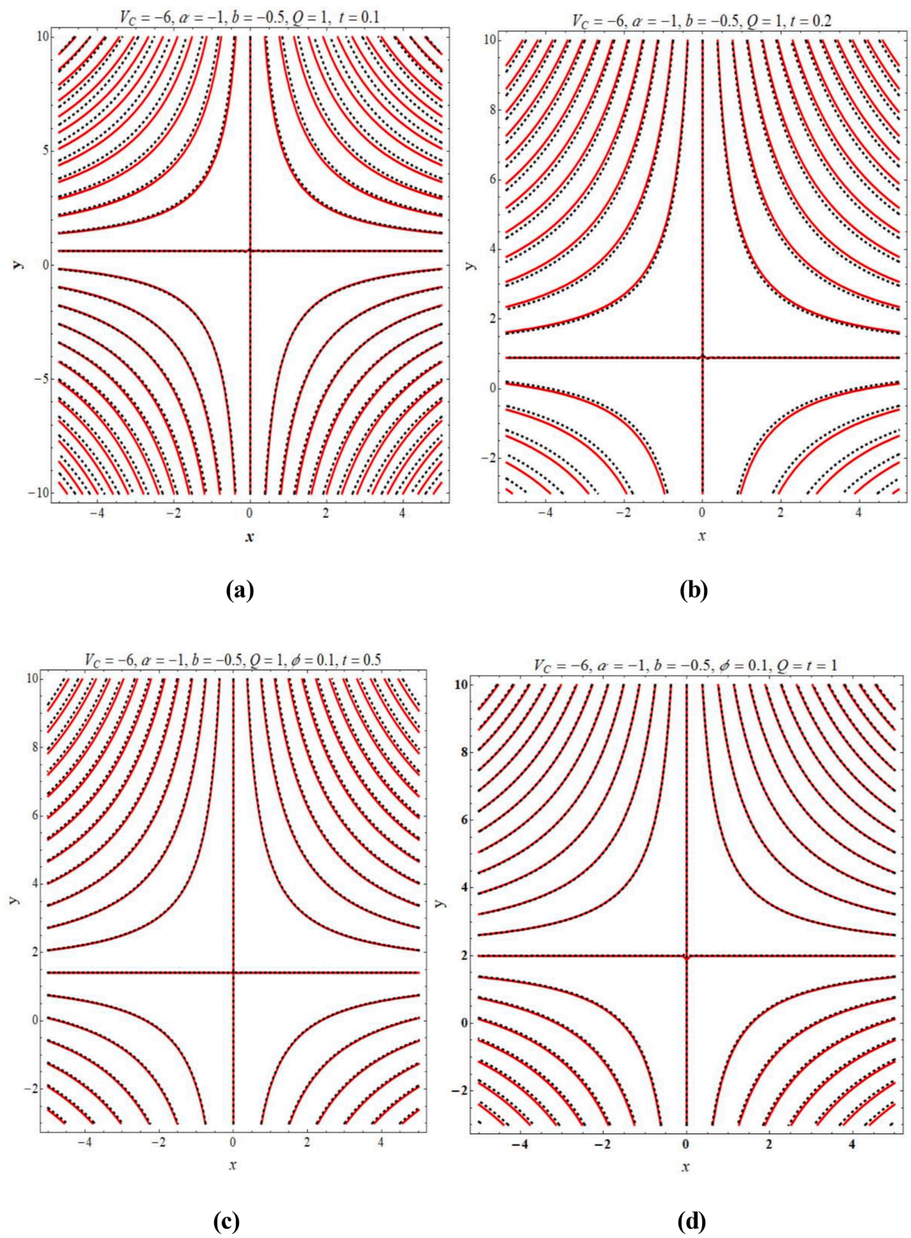

Fig. 5. Streamline patterns at different time for lower branch of solution.

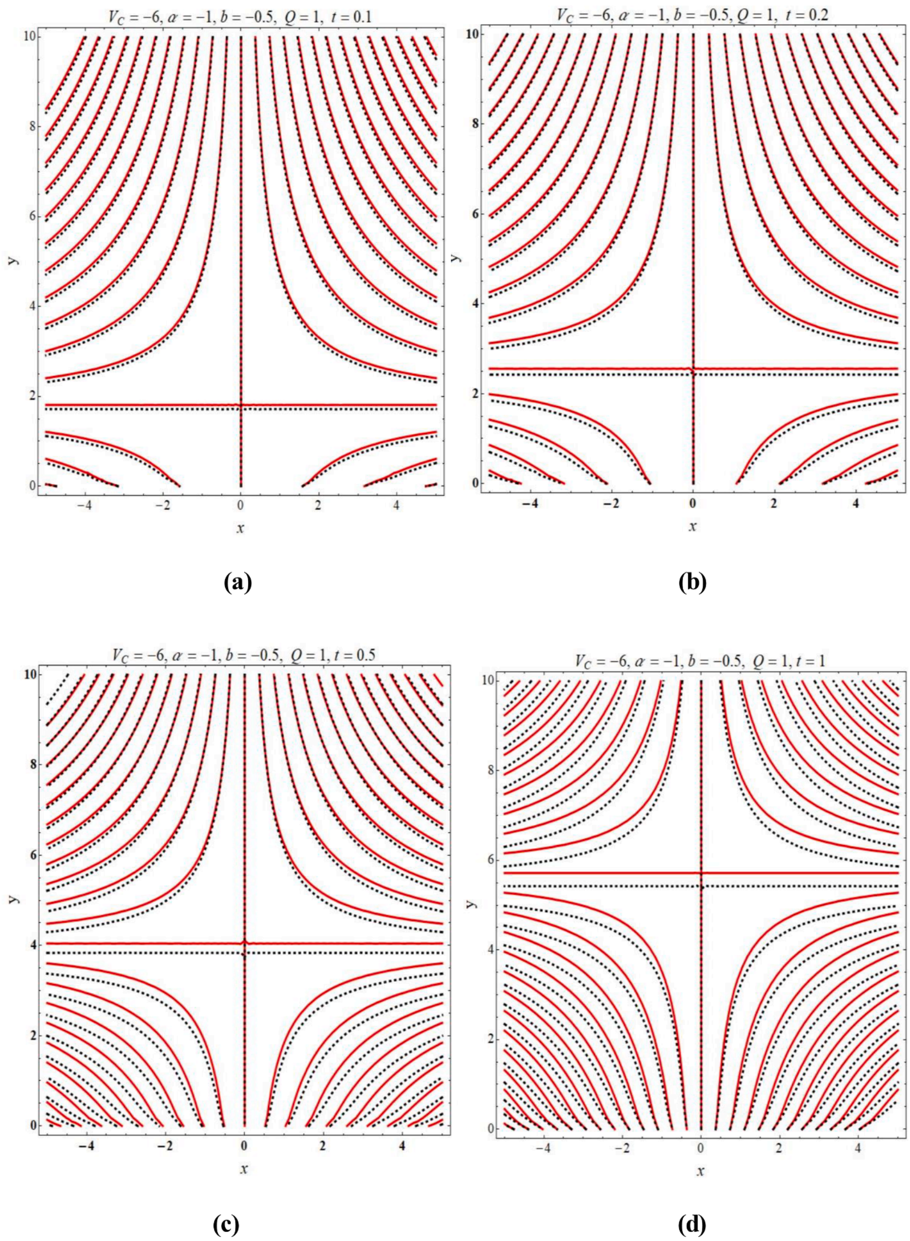

Fig. 6. streamline patterns at different time for upper branch of solution.

Also we got

$$2\varepsilon_1\beta^2+\varepsilon_2V_C\beta+(\varepsilon_2(\alpha+3)-2\varepsilon_3Q)=0 \tag{20}$$

The answer to this quadratic equation is as follows.

$$\beta=\frac{-\varepsilon_2V_C+\sqrt{(\varepsilon_2V_C)^2-8\varepsilon_1(\varepsilon_2(\alpha+3)-2\varepsilon_2)}}{4\varepsilon_1} \tag{21}$$

here, β must be positive value for physically feasible solution. Based on Eq. (20) the real roots can be yield only when the V_C and α must satisfy $(\varepsilon_2V_C)^2-8\varepsilon_1(\varepsilon_2(\alpha+3)-2\varepsilon_2)\geqslant 0$.It is observed that there are two solutions for Eq.(20) for certain values of V_C and α.The general solution for Eq.(15) is given for upper solution branch

$$f(\eta)=\eta+V_C+\frac{4\varepsilon_1(1-\alpha)}{-\varepsilon_2V_C+\sqrt{\sqrt{(\varepsilon_2V_C)^2-8\varepsilon_1(\varepsilon_2(\alpha+3)-2\varepsilon_2)}}}\times\left(Exp\left(-\frac{-\varepsilon_2V_C+\sqrt{\sqrt{(\varepsilon_2V_C)^2-8\varepsilon_1(\varepsilon_2(\alpha+3)-2\varepsilon_2)}}}{4\varepsilon_1}\eta\right)-1\right) \tag{22}$$

And for the lower solution branch is given by

$$f(\eta)=\eta+V_C+\frac{4\varepsilon_1(1-\alpha)}{-\varepsilon_2V_C-\sqrt{\sqrt{(\varepsilon_2V_C)^2-8\varepsilon_1(\varepsilon_2(\alpha+3)-2\varepsilon_2)}}}\times\left(Exp\left(-\frac{-\varepsilon_2V_C-\sqrt{\sqrt{(\varepsilon_2V_C)^2-8\varepsilon_1(\varepsilon_2(\alpha+3)-2\varepsilon_2)}}}{4\varepsilon_1}\eta\right)-1\right) \tag{23}$$

And the velocity for upper and lower branch solution is given by

$$f(\eta)=1+(\alpha-1)Exp\left(-\frac{-\varepsilon_2V_C+\sqrt{\sqrt{(\varepsilon_2V_C)^2-8\varepsilon_1(\varepsilon_2(\alpha+3)-2\varepsilon_2)}}}{4\varepsilon_1}\eta\right) \tag{24}$$

$$f(\eta)=1+(\alpha-1)Exp\left(-\frac{-\varepsilon_2V_C+\sqrt{\sqrt{(\varepsilon_2V_C)^2-8\varepsilon_1(\varepsilon_2(\alpha+3)-2\varepsilon_2)}}}{4\varepsilon_1}\eta\right) \tag{25}$$

5. Analytical solution of energy equation

Applying the similarity variables to Eq. (4), we obtain the following ODE

$$(\varepsilon_5+R)\theta_{\eta\eta}+Pr\varepsilon_4\left(\frac{\eta}{2}+bf\right)\theta_\eta=0 \tag{26}$$

For the PST and PHF cases, the boundary conditions associated with this energy equation are reduced to the following form.

$$\left.\begin{matrix}\theta(0)=1,\ \theta(\infty)\to 0 \quad \text{for PST case}\\ h_\eta(0)=-1,\ h(\infty)\to 0 \quad \text{for PHF case}\end{matrix}\right\} \tag{27a,b}$$

here, $Pr=\frac{(\mu C_P)_f}{\kappa_f}$ is Prandtl number, $R=\frac{16\sigma^* T_\infty^3}{3K_f k^*}$ is the radiation parameter, it is computed with the use of Rosseland's approximation, using this estimation q_r is modelled as $q_r=-\frac{4\sigma^*}{3k^*}\frac{\partial T^4}{\partial y}$, then it is possible to expand the word T^4 using Taylor's series while disregarding higher order terms to obtain $T^4=-3T_\infty^3+4T_\infty^3T$. on substituting these terms into Eq. (4) to get $\frac{\partial q_r}{\partial y}=-\frac{16\sigma^* T_\infty^3}{3k^*}\frac{\partial^2 T}{\partial y^2}$, by using this the thermal radiation R can be calculated (See Mahabaleshwar et al. [25–27,34–36]). Also nanofluid quantities ε_1 to ε_5 used in Eq.(14) and (26) is given by (See [28–29,37–39])

$$\varepsilon_1=\frac{\mu_{nf}}{\mu_f}=\frac{1}{(1-\phi)^{2.5}} \tag{28a}$$

$$\varepsilon_2=\frac{\rho_{nf}}{\rho_f}=1-\phi+\phi\frac{\rho_s}{\rho_f} \tag{28b}$$

$$\varepsilon_3=\frac{\sigma_{nf}}{\sigma_f}=1+\frac{3\left(\frac{\sigma_s}{\sigma_f}-1\right)\phi}{\left(\frac{\sigma_s}{\sigma_f}+2\right)-\left(\frac{\sigma_s}{\sigma_f}-1\right)\phi} \tag{28c}$$

$$\varepsilon_4=\frac{(\rho C_P)_{nf}}{(\rho C_P)_f}=1-\phi+\phi\frac{(\rho C_p)_s}{(\rho C_p)_f} \tag{28d}$$

$$\varepsilon_5=\frac{\kappa_{nf}}{\kappa_f}=\frac{\kappa_s+2\kappa_f+2\phi(\kappa_s-\kappa_f)}{\kappa_s+2\kappa_f-\phi(\kappa_s-\kappa_f)}. \tag{28e}$$

Then by using Eq.(20) the term V_C can be obtained as

$$V_C=\frac{-2\varepsilon_1}{\varepsilon_2}\beta-\frac{(\varepsilon_2(\alpha+3)-2\varepsilon_3Q)}{\beta\varepsilon_2} \tag{29}$$

5.1. Constant wall temperature case (PST case)

By using Eq. (29) the energy equation can be altered as

$$(\varepsilon_5+R)\theta_{\eta\eta}-\frac{1}{2}Pr\varepsilon_4\left(V_C-\frac{(1-\alpha)}{\beta}+\frac{(1-\alpha)}{\beta}Exp(-\beta\eta)\right)\theta_\eta=0 \tag{30}$$

Introducing a new variable ξ as

$$\xi=(1-\alpha)\frac{Pr}{2\beta^2}Exp(-\beta\eta) \tag{31}$$

using new transformation ξ and V_C in Eq.(30) to yield the following resulting equation

$$\xi(\varepsilon_5+R)\frac{\partial^2\theta}{\partial\xi^2}+\left((\varepsilon_5+R)-\varepsilon_4Pr\left(\frac{\varepsilon_1}{\varepsilon_2}+\frac{2\varepsilon_2-\varepsilon_3Q}{\beta^2}\right)+\varepsilon_4\xi\right)\frac{\partial\theta}{\partial\xi}=0 \tag{32}$$

Boundary conditions associated with PST case is also reduces to

$$\theta\left(\frac{Pr(1-\alpha)}{2\beta^2}\right)=1,\quad \theta(0)=0 \tag{33}$$

Then the general solution of Eq. (32) gives as

$$\theta(\xi)=C_1+C_2\frac{\frac{Pr}{(\varepsilon_5+R)}\left(\frac{\varepsilon_1}{\varepsilon_2}+\frac{2\varepsilon_2-\varepsilon_3Q}{\beta^2}\right)}{\varepsilon_4^{\frac{Pr}{(\varepsilon_5+R)}\left(\frac{\varepsilon_1}{\varepsilon_2}+\frac{2\varepsilon_2-\varepsilon_3Q}{\beta^2}\right)}}\Gamma\left(\frac{Pr}{(\varepsilon_5+R)}\left(\frac{\varepsilon_1}{\varepsilon_2}+\frac{2\varepsilon_2-\varepsilon_3Q}{\beta^2}\right),0\right)-\Gamma\left(\frac{Pr}{(\varepsilon_5+R)}\left(\frac{\varepsilon_1}{\varepsilon_2}+\frac{2\varepsilon_2-\varepsilon_3Q}{\beta^2}\right),\varepsilon_4\xi\right) \tag{34}$$

By using the boundary condition defined at Eq.(27a) in Eq. (34) to yield the following result

$$\theta(\eta)=\frac{\Gamma\left[\frac{Pr}{(\varepsilon_5+R)}\left(\frac{\varepsilon_1}{\varepsilon_2}+\frac{2\varepsilon_2-\varepsilon_3Q}{\beta^2}\right),0\right]-\Gamma\left[\frac{Pr}{(\varepsilon_5+R)}\left(\frac{\varepsilon_1}{\varepsilon_2}+\frac{2\varepsilon_2-\varepsilon_3Q}{\beta^2}\right),\varepsilon_4\frac{(1-\alpha)Pr}{2\beta^2}Exp(-\beta\eta)\right]}{\Gamma\left[\frac{Pr}{(\varepsilon_5+R)}\left(\frac{\varepsilon_1}{\varepsilon_2}+\frac{2\varepsilon_2-\varepsilon_3Q}{\beta^2}\right),0\right]-\Gamma\left[\frac{Pr}{(\varepsilon_5+R)}\left(\frac{\varepsilon_1}{\varepsilon_2}+\frac{2\varepsilon_2-\varepsilon_3Q}{\beta^2}\right),\varepsilon_4\frac{(1-\alpha)Pr}{2\beta^2}\right]} \tag{35}$$

then the wall's heat flux is determined by

$$\theta_\eta(0)=\frac{-\beta\left(\frac{(1-\alpha)Pr}{2\beta^2}\right)^{\frac{Pr}{(\varepsilon_5+R)}\left(\frac{\varepsilon_1}{\varepsilon_2}+\frac{2\varepsilon_2-\varepsilon_3 Q}{\beta^2}\right)}Exp\left(-\frac{(1-\alpha)Pr}{2\beta^2}\right)}{\Gamma\left[\frac{Pr}{(\varepsilon_5+R)}\left(\frac{\varepsilon_1}{\varepsilon_2}+\frac{2\varepsilon_2-\varepsilon_3 Q}{\beta^2}\right),\ 0\right]-\Gamma\left[\frac{Pr}{(\varepsilon_5+R)}\left(\frac{\varepsilon_1}{\varepsilon_2}+\frac{2\varepsilon_2-\varepsilon_3 Q}{\beta^2}\right),\ \varepsilon_4\frac{(1-\alpha)Pr}{2\beta^2}\right]}\tag{36}$$

5.2. Uniform heat flux case

Defining $h(\eta)=\frac{T-T_\infty}{\frac{q_w}{\kappa}\sqrt{\nu}}$, adding this to the energy equation will provide the following equation:

$$(\varepsilon_5+R)h_{\eta\eta}+\frac{1}{2}\varepsilon_4 Pr(\eta-f)h_\eta=0\tag{37}$$

using solution of momentum in Eq. (37) to yield

$$(\varepsilon_5+R)h_{\eta\eta}-\frac{1}{2}Pr\varepsilon_4\left(V_C-\frac{(1-\alpha)}{\beta}+\frac{(1-\alpha)}{\beta}Exp(-\beta\eta)\right)h_\eta=0\tag{38}$$

Since Eq. (38) and Eq. (30) are comparable, and Eq. (34) and Eq. (30) have the same solution, the general answer to Eq. (38) is obtained as

$$h(\xi)=C_1+C_2\frac{\frac{Pr}{(\varepsilon_5+R)}\left(\frac{\varepsilon_1}{\varepsilon_2}+\frac{2\varepsilon_2-\varepsilon_3 Q}{\beta^2}\right)}{\varepsilon_4^{\frac{Pr}{(\varepsilon_5+R)}\left(\frac{\varepsilon_1}{\varepsilon_2}+\frac{2\varepsilon_2-\varepsilon_3 Q}{\beta^2}\right)}}$$

$$\Gamma\left(\frac{Pr}{(\varepsilon_5+R)}\left(\frac{\varepsilon_1}{\varepsilon_2}+\frac{2\varepsilon_2-\varepsilon_3 Q}{\beta^2}\right),0\right)-\Gamma\left(\frac{Pr}{(\varepsilon_5+R)}\left(\frac{\varepsilon_1}{\varepsilon_2}+\frac{2\varepsilon_2-\varepsilon_3 Q}{\beta^2}\right),\varepsilon_4\xi\right)\tag{39}$$

By incorporating the boundary conditions from Eq. (27b) into Eq. (39), the following equation is produced.

$$h(\eta)=\frac{\Gamma\left[\frac{Pr}{(\varepsilon_5+R)}\left(\frac{\varepsilon_1}{\varepsilon_2}+\frac{2\varepsilon_2-\varepsilon_3 Q}{\beta^2}\right),\ 0\right]-\Gamma\left[\frac{Pr}{(\varepsilon_5+R)}\left(\frac{\varepsilon_1}{\varepsilon_2}+\frac{2\varepsilon_2-\varepsilon_3 Q}{\beta^2}\right),\ \varepsilon_4\frac{(1-\alpha)Pr}{2\beta^2}Exp(-\beta\eta)\right]}{\beta\left(\frac{(1-\alpha)Pr}{2\beta^2}\right)^{\frac{Pr}{(\varepsilon_5+R)}\left(\frac{\varepsilon_1}{\varepsilon_2}+\frac{2\varepsilon_2-\varepsilon_3 Q}{\beta^2}\right)}Exp\left(-\frac{(1-\alpha)Pr}{2\beta^2}\right)}\tag{40}$$

Given as follows is the dimensionless wall heat flux:

$$h(0)=\frac{\Gamma\left[\frac{Pr}{(\varepsilon_5+R)}\left(\frac{\varepsilon_1}{\varepsilon_2}+\frac{2\varepsilon_2-\varepsilon_3 Q}{\beta^2}\right),\ 0\right]-\Gamma\left[\frac{Pr}{(\varepsilon_5+R)}\left(\frac{\varepsilon_1}{\varepsilon_2}+\frac{2\varepsilon_2-\varepsilon_3 Q}{\beta^2}\right),\ \varepsilon_4\frac{(1-\alpha)Pr}{2\beta^2}\right]}{\beta\left(\frac{(1-\alpha)Pr}{2\beta^2}\right)^{\frac{Pr}{(\varepsilon_5+R)}\left(\frac{\varepsilon_1}{\varepsilon_2}+\frac{2\varepsilon_2-\varepsilon_3 Q}{\beta^2}\right)}Exp\left(-\frac{(1-\alpha)Pr}{2\beta^2}\right)}\tag{41}$$

On the analysis of this result, it is observed that $h(0)=-\frac{1}{\theta_\eta(0)}$.

5.3. Power law wall temperature for general case

The conditions used in the above literature is very rare to investigate the temperature at wall. But in this section we discussed the general situation by taking power law depended on both time and distance and it is given by

$$T=T_\infty+(T_w-T_\infty)x^n t^m\theta(\eta)\tag{42}$$

$$-\theta_\eta(0)=\delta\beta+\frac{(\alpha-1)(\delta-n)Pr}{\beta(\varepsilon_5+R)(2(\varepsilon_5+R)-A+2\delta(\varepsilon_5+R))}\frac{M\left(\delta-n+1,\ \gamma+1,\ \frac{(\alpha-1)Pr}{2(\varepsilon_5+R)\beta^2}\right)}{M\left(\delta-n,\ \gamma,\ \frac{(\alpha-1)Pr}{2(\varepsilon_5+R)\beta^2}\right)}\tag{54}$$

The following ODE, which has no relation to Eq. (4), is obtained by substituting this new definition into Eq. (26)

$$(\varepsilon_5+R)\theta_{\eta\eta}+\varepsilon_4 Pr\left(bf+\frac{1}{2}\eta\right)\theta_\eta-\varepsilon_4 Pr(bnf_\eta+m)\theta=0\tag{43}$$

The boundary conditions associated with Eq. (43) as

$$\theta(0)=1,\ \ \theta(\infty)=0\tag{44}$$

Put $b=-1/2$ in Eq.(43), then Eq.(43) becomes

$$(\varepsilon_5+R)\theta_{\eta\eta}+\varepsilon_4\frac{Pr}{2}(\eta-f)\theta_\eta+\varepsilon_4\frac{Pr}{2}(nf_\eta-2m)\theta=0\tag{45}$$

using $\xi=\frac{(\alpha-1)}{2Pr\beta^2}Exp(-\beta\eta)$ in Eq.(45) to yield as

$$\xi(\varepsilon_5+R)\frac{\partial^2\theta}{\partial\xi^2}+((\varepsilon_5+R)-A-\xi)\frac{\partial\theta}{\partial\xi}+\left(\frac{B}{\xi}+n\right)\theta=0\tag{46}$$

here, $A=Pr\varepsilon_4\left(1+\frac{2\varepsilon_2-\varepsilon_3 M}{\beta^2}\right)$, $B=\frac{1}{\beta^2}Pr\varepsilon_4\left(\frac{n}{2}-m\right)$.

Boundary conditions defined in Eq. (44) reduces as

$$\theta\left(\frac{Pr(\alpha-1)}{2\beta^2}\right)=1,\ \ \theta(0)=0\tag{47}$$

Now we define

$$\theta(\xi)=\xi^\delta\psi(\xi)\tag{48}$$

On applying Eq. (48) in Eq. (46), then it transformed as

$$\xi(\varepsilon_5+R)\frac{\partial^2\psi}{\partial\xi^2}+(\gamma-\xi)\frac{\partial\psi}{\partial\xi}+\left\{\frac{1}{\xi}\left(\delta^2(\varepsilon_5+R)-A\delta+B\right)-\delta+n\right\}\psi(\xi)=0\tag{49}$$

here, $\delta=\frac{A\pm\sqrt{A^2-4B(\varepsilon_5+R)}}{2(\varepsilon_5+R)}$, which requires $A^2-4B(\varepsilon_5+R)\geqslant 0$, and $\frac{Pr\varepsilon_4}{\beta^2}\left(\beta^2\varepsilon_1+2\varepsilon_2-\varepsilon_3 Q\right)^2\geqslant 2n-4m$, with $\omega=\delta-n$.

Therefore, Eq. (49) becomes

$$\xi(\varepsilon_5+R)\frac{\partial^2\psi}{\partial\xi^2}+(\gamma-\xi)\frac{\partial\psi}{\partial\xi}-\omega\psi(\xi)=0\tag{50}$$

Given that Eq. (50) is a basic confluent hypergeometric differential equation, the following is its solution:

$$\psi(\xi)=C_1 M\left(\omega,\gamma,\frac{\xi}{(\varepsilon_5+R)}\right)\tag{51}$$

By using the boundary condition $\theta(0)=1$ the constant C_1 can be determined

$$C_1=\frac{\left((\alpha-1)\frac{Pr}{2\beta^2}\right)^{-\delta}}{M\left(\omega,\gamma,\frac{(\alpha-1)Pr}{2(\varepsilon_5+R)\beta^2}\right)}\tag{52}$$

then using $\psi(\xi)$ in Eq.(48) to yield the result as

$$\theta(\eta)=\frac{Exp(-\beta\delta\eta)M\left(\delta-n,\ \gamma,\ \frac{(\alpha-1)Pr}{2(\varepsilon_5+R)\beta^2}Exp(-\beta\eta)\right)}{M\left(\delta-n,\ \gamma,\ \frac{(\alpha-1)Pr}{2(\varepsilon_5+R)\beta^2}\right)}\tag{53}$$

The wall heat flux is then presented as

5.4. Power law heat flux for general case

Let us assume that power law heat flux at wall heat flux depended on both time and distance as

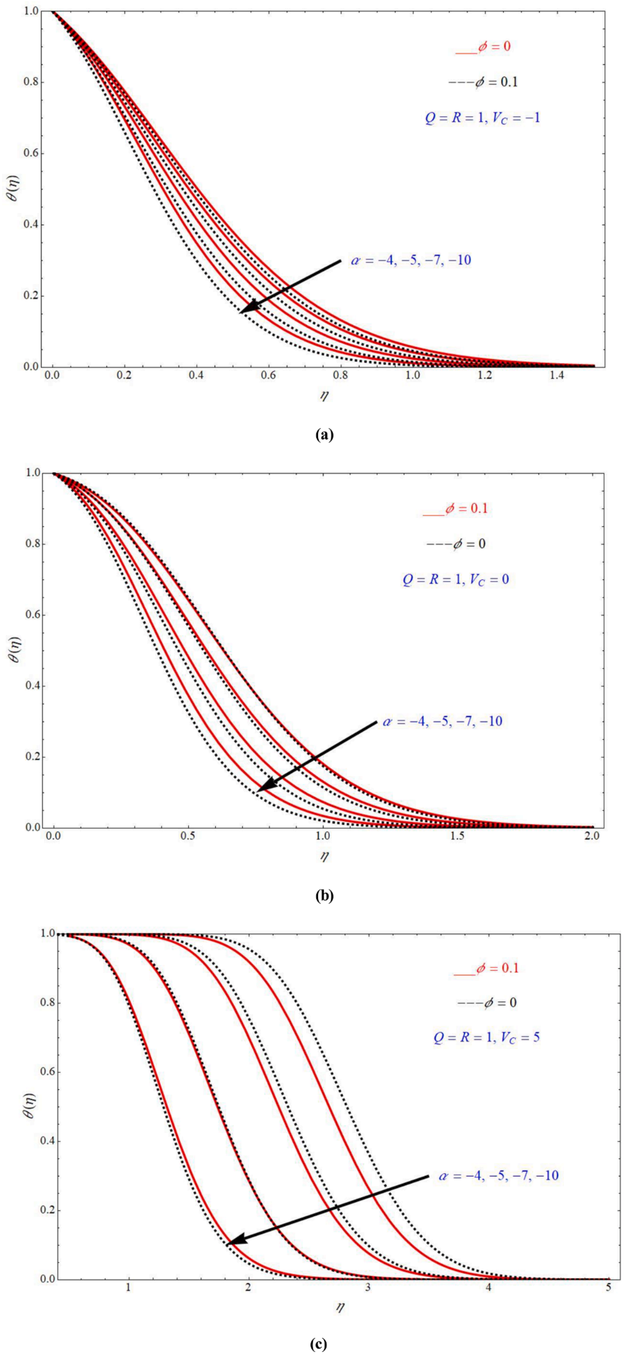

Fig. 7. Impact of $\theta(\eta)$ on η for various α values at (a) injection ($V_C < 0$)(b) no permeability ($V_C = 0$) and (c) suction ($V_C > 0$).

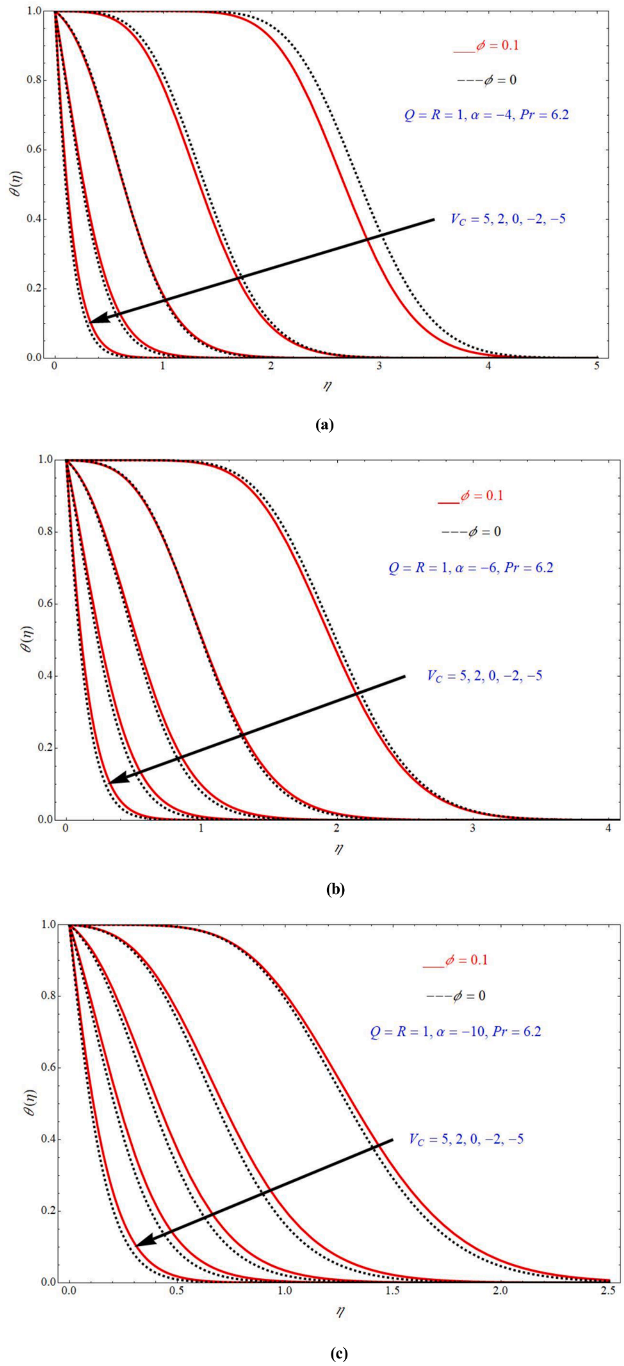

Fig. 8. Impact of $\theta(\eta)$ on η for various V_C values at (a) $\alpha = -4$(b) $\alpha = -6$(c) $\alpha = -10$ and (d) $\alpha = -12$.

$$-\kappa\frac{\partial T}{\partial y} = q_w x^n t^{m-\frac{1}{2}} \tag{55}$$

therefore, dimensionless temperature is given by

$$T = T_\infty + \frac{q_w}{\kappa}\sqrt{\nu}x^n t^m h(\eta) \tag{56}$$

when this is substituted into Equation (4), the resulting equation is

$$(\varepsilon_5 + R)h_{\eta\eta} + \varepsilon_4 Pr\left(bf + \frac{1}{2}\eta\right)h_\eta - \varepsilon_4 Pr(bnf_\eta + m)h = 0 \tag{57}$$

consider $b = -1/2$ in Eq.(57) then it is changed as

$$(\varepsilon_5 + R)h_{\eta\eta} + \varepsilon_4\frac{Pr}{2}(\eta - f)h_\eta + \varepsilon_4\frac{Pr}{2}(nf_\eta - 2m)h = 0 \tag{58}$$

The associated boundary conditions of Eq. (58) reduced to

$$h_\eta(0) = -1, \quad h(\infty) \rightarrow 0 \tag{59}$$

Since Eq. (58) is similar to Eq. (45) in this case and the answer up to Eq. (51) is identical to Eq. (45), the solution to Eq. (58) is given by

$$\psi(\xi) = C_1 M\left(\omega, \gamma, \frac{\xi}{(\varepsilon_5 + R)}\right) \tag{60}$$

The boundary conditions stated in Eq. (59) allow the determination of C_1

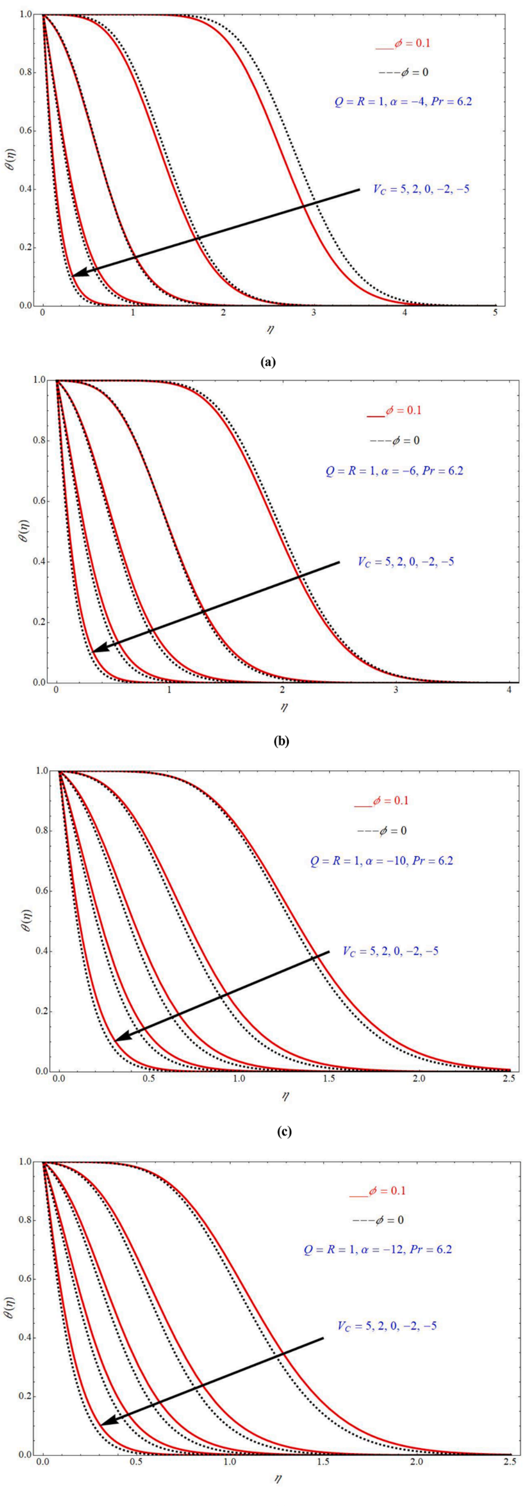

Fig. 9. Impact of $-\theta_\eta(0)$ on R, as a function of (a) V_C(b) Pr.

$$C_1 = \frac{\left(\frac{(\alpha-1)Pr}{2\beta^2}\right)^{-1}}{\left\{\delta\beta M\left(\omega,\ \gamma,\ \frac{(\alpha-1)Pr}{2(\varepsilon_5+R)\beta^2}\right) + \frac{\omega Pr(\alpha-1)}{2\beta\gamma} M\left(\omega+1,\ \gamma+1,\ \frac{(\alpha-1)Pr}{2(\varepsilon_5+R)\beta^2}\right)\right\}} \tag{61}$$

Using C_1 in Eq. (60) to get

$$h(\eta) = \frac{Exp(-\beta\delta\eta) M\left(\omega,\ \gamma,\ \frac{(\alpha-1)Pr}{2(\varepsilon_5+R)\beta^2} Exp(-\beta\eta)\right)}{\left\{\delta\beta M\left(\omega,\ \gamma,\ \frac{(\alpha-1)Pr}{2(\varepsilon_5+R)\beta^2}\right) + \frac{\omega Pr(\alpha-1)}{2\beta\gamma} M\left(\omega+1,\ \gamma+1,\ \frac{(\alpha-1)Pr}{2(\varepsilon_5+R)\beta^2}\right)\right\}} \tag{62}$$

$$h(0) = \frac{M\left(\omega,\ \gamma,\ \frac{(\alpha-1)Pr}{2(\varepsilon_5+R)\beta^2}\right)}{\left\{\delta\beta M\left(\omega,\ \gamma,\ \frac{(\alpha-1)Pr}{2(\varepsilon_5+R)\beta^2}\right) + \frac{\omega Pr(\alpha-1)}{2\beta\gamma} M\left(\omega+1,\ \gamma+1,\ \frac{(\alpha-1)Pr}{2(\varepsilon_5+R)\beta^2}\right)\right\}} \tag{63}$$

6. Results and discussion

Results obtained from the 2-D unsteady fluid flow with transpiration and radiation is analysed using different controlling parameters. Velocity equation is solved exactly to yield solution domain, here the dual nature characteristics. This domain helps to solve the heat equation and also put this in terms of incomplete gamma function and also in terms of confluent hypergeometric equation.

6.1. Discussion for flow problem

The plots of β verses α for different V_C at $Q = 0$ and $Q = 1$ respectively studied at Fig. 2a and b, here domain move towards the positive values of α if we decreases the values of mass transpiration V_C. The solution domain is little bit more value for $Q = 1$, compare to $Q = 0$. For $V_C \geqslant 0$, there is one solution for $\alpha = -3$. The flow problem exist two solution for $V_C < 0$. Fig. 3a and b represents the effect of $f_\eta(\eta)$ on η for different V_C, at $\alpha = -4$, and $\alpha = -8$, respectively. These two plots represent the shrinking sheet case because $\alpha < 0$ here the velocity decays on raising the V_C values. Impact of mass transpiration V_C on velocity is represented at Fig. 4a and b for upper branch of solution(*ubs*) and lower branch of solution (*lbs*) respectively, red lines depict *ubs* and black lines depict *lbs*. Fig. 4a indicates shrinking sheet case because $\alpha = -1$, here velocity decays on raising the values of V_C for upper branch of solution and increases with increases of V_C for lower branch of solution. Similarly, Fig. 4b depict the stretching sheet case because $\alpha = 2$. In this velocity increases with increase of V_C for upper branch of solution and decreases with increase of V_C for lower branch of solution. In these figures dotted lines for $\phi = 0$, and solid lines for $\phi = 0.1$. Fig. 5a to d depict the pattern of stream lines for lower branch of solution at varying time. On the basis of the definitions the formula of stream function is given by

$$\psi(x, y, t) = -\frac{1}{2} f\left(\frac{y}{t}\right) x \sqrt{\frac{1}{t}}$$

Fig. 6a–d depict the pattern of stream lines for upper branch of solution at different time. From these two branches it is cleared that stagnation points of upper and lower solution branch moving away from the wall.

6.2. Discussion for energy equation

Energy equation is discussed under four different cases, these cases are examined analytically, these analytical results are verified with graphical arrangements. Figs. 7–9 graphs are related to constant wall temperature case. Fig. 7a–c depicts the plots of $\theta(\eta)$ verses η for different α values respectively at injection ($V_C < 0$), no-permeability ($V_C = 0$) and suction ($V_C > 0$). Here $\theta(\eta)$ raises for raising the values of α for all the cases of injection, no-permeability and suction. The boundary value thickness is more wider for large values of V_C. Effect of $\theta(\eta)$ on η for various choices of V_C at different $\alpha = -4, -6, -10, -12$ respectively indicated at Fig. 8a–d. Here $\theta(\eta)$ raises for raising the values of V_C. Fig. 9a–b depicts the effect of $-\theta_\eta(0)$ on R as a function of V_C and Pr, respectively. In both conditions the value of R more for more values of Pr

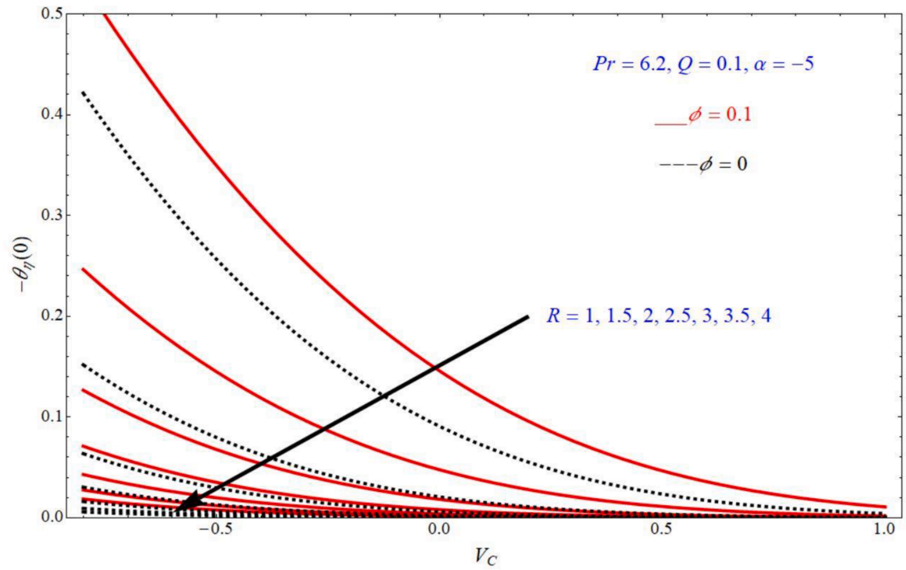

(a)

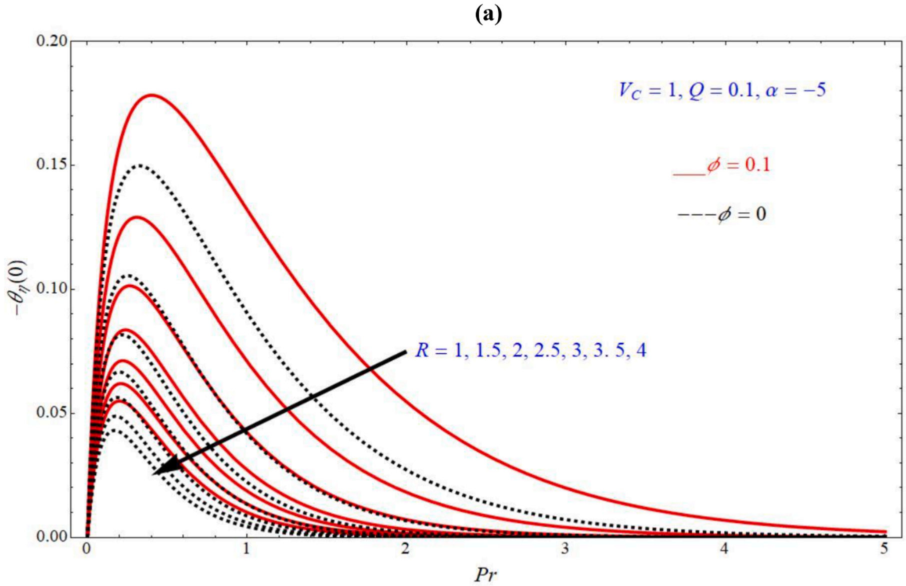

(b)

Fig. 10. $h(\eta)$ verses η for various α values at (a) injection (b) no permeability and (c) suction.

and V_C, also the value of $-\theta_\eta(0)$ increases with decreases the values of R. Fig. 10a to c are related to the uniform heat flux case, these graphs portrays plots of $h(\eta)$ on η for various choices of α at injection ($V_C < 0$), no-permeability ($V_C = 0$) and suction ($V_C > 0$) cases respectively. In all the three cases $h(\eta)$ increases for increases the values of α. Fig. 11 exhibit the result of general power-law walls temperature case, it is mathematically represented at Eq. (53). Fig. 11a–c portrays general power-law surface temperature $\theta(\eta)$ on η for different values of m, at $n = -15, -10, -5$ respectively. From these figures it is cleared that the values of m decays the temperature profile value, also boundary value thickness is more wider for more values of n.

7. Concluding remarks

The current work investigates the two-dimensional unsteady stagnation point flow with G-H_2O nanoparticles. Velocity and heat equations solved exactly, then the heat equation solved under PST and PHF conditions. The energy equations are also solved under four different cases and represented in terms of incomplete gamma function as well as Kummer's function to provide the solution domain for the resultant ODEs. Analysing the results of the present can be done by employing different regulating parameters. The flow's dual nature can also be verified. It is possible to draw conclusions from the results using graphical representations. At the end we get the following results.

- The solution domain of the momentum equation containing two branches of solution namely upper and lower branches.
- Domain value raises for raising the V_C values. Here domain is little bit more value for $Q = 1$, compare to $Q = 0$.
- Velocity decreases with increases of V_C for *ubs* and increases with increases of V_C for lower branch of solution in the case shrinking sheet.
- Velocity decreases with increases of V_C for upper branch of solution and increases with increases of V_C for lower branch of solution in the case of stretching sheet.

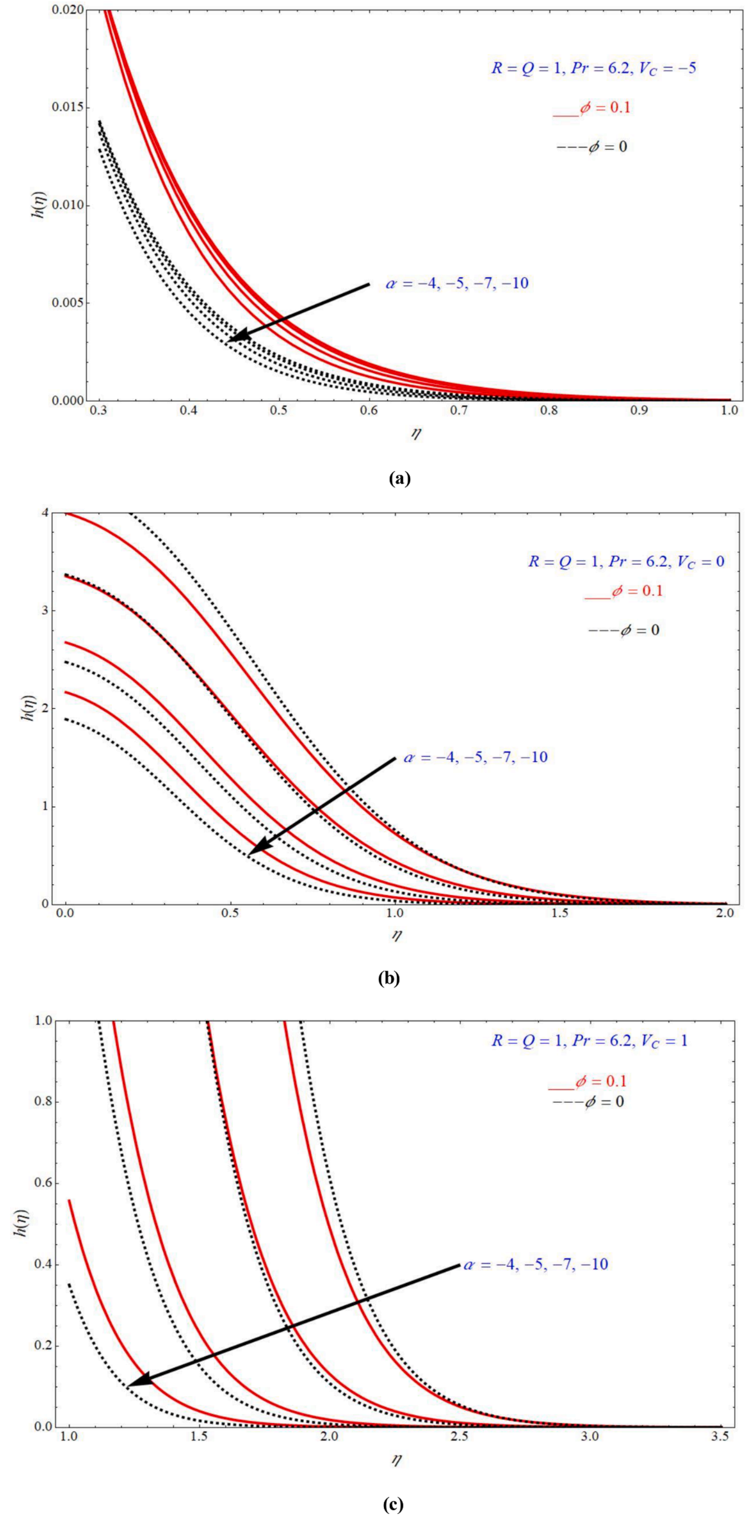

Fig. 11. Impact of general power-law surface temperature $\theta(\eta)$ on η for various m values at (a) $n = -15$(b) $n = -10$ and (c) $n = -5$.

- $\theta(\eta)$ raises for raising α and V_C values for all the cases of injection, no-permeability and suction.
- In the case constant power law wall temperature the value of R decays on raising Pr and V_C, also the value of $-\theta_\eta(0)$ increases with decreases the values of R
- $h(\eta)$ raises for raising the values of α in the case of uniform heat flux case.
- In the case of general power-law walls temperature, values of m decreases the temperature profile value.

CRediT authorship contribution statement

A.B. Vishalakshi: Conceptualization, Investigation, Methodology, Writing – review & editing. **U.S. Mahabaleshwar:** Supervision, Conceptualization, Methodology, Formal analysis, Writing – original draft. **L.M. Pérez:** Methodology, Writing – review & editing. **O. Manca:** Supervision, Methodology, Writing – review & editing.

Declaration of Competing Interest

The authors declare that they have no known competing financial interests or personal relationships that could have appeared to influence the work reported in this paper.

Data availability

Data will be made available on request.

Acknowledgments

L.M.P. acknowledges partial financial support from ANID through *Convocatoria Nacional Subvención a Instalación en la Academia Convocatoria Año 2021*, Grant SA77210040. Dr. U.S. Mahabaleshwar is thankful to University of Tarapaca for his hospitality during his stay at the University of Tarapaca, Chile.

References

[1] M.M. Amin, M.H. Ahmadi, M.B. Fatemeh Joda, V. Antonio, S. Uson, Exergy analysis of a Combined Cooling Heating and power system integrated with wind turbine and compressed air energy storage system, Eng. Conv. Manage. 131 (2017) 69–78.
[2] B.C. Sakiadis, Boundary-layer behavior on continuous solid surface, AIChE J. 7 (1961) 26–28.
[3] B.C. Sakiadis, Boundary-layer behavior on continuous solid surfaces. II. The boundary layer on a continuous flat surface AIChE J. 7(1961b) 221–225.
[4] L.J. Crane, Flow past a stretching plate, Z. Angew. Math. Phys. 21 (1970) 645–647.
[5] E.H. Aly, Existence of the multiple exact solutions for nanofluids flow over a stretching/shrinking sheet embedded in a porous medium at the presence of magnetic field with electrical conductivity and thermal radiation effects, Powder Tech. 301 (2016) 760–781.
[6] U.S. Mahabaleshwar, K.R. Nagaraju, P.N. Vinay Kumar, D. Baleanu, G. Lorenzini, An exact analytical solution of the unsteady magnetohydrodynamics nonlinear dynamics of laminar boundary layer due to an impulsively linear stretching sheet, continuum, Mech Thermodyn 29 (2017) 559–567.
[7] H.I. Andersson, K.H. Bech, B.S. Dandapat, Magnetohydrodynamic flow of a power-law fluid over a stretching sheet, Int. J. Non Linear Mech. 27 (1992) 929–936.
[8] H.I. Andersson, MHD flow of a viscoelastic fluid past a stretching surface, Acta Mechanica 95 (1992) 227–230.
[9] U.S. Mahabaleshwar, K.R. Nagaraju, M.A. Sheremet, P.N. Vinay Kumar, G. Lorenzini, Effect of mass transfer and MHD inclined Navier's slip flow due to non-linear stretching sheet, J. Eng. Thermophysics. 28 (2019) 578–590.
[10] U.S. Mahabaleshwar, G. Lorenzini, Combined effect of heat source/sink and stress work on MHD Newtonian fluid flow over a stretching porous sheet, Int. J. Heat Technol. 35 (2017) 330–335.
[11] U.S. Mahabaleshwar, M.B. Rekha, P.N. Vinay Kumar, F. Selimefendigil, P. H. Sakanaka, G. Lorenzini, S.N. Ravichandra Nayakar, Mass transfer characteristics of MHD Casson fluid flow past stretching/shrinking sheet, J. Eng. Therm. Phys. 29 (2020) 285–302.
[12] U.S. Mahabaleshwar, I. Pažanin, M. Radulović, F.J. Suarez-Grau, Effects of small boundary perturbation on the MHD duct flow, Theor. Appl. Mech. 44 (1) (2017) 83–101.
[13] S.U.S. Choi, Enhancing thermal conductivity of fluids with nanoparticle, Proc. ASME Int. Mech. Eng. Congress Exposition 66 (1995) 99–105.
[14] U.S. Mahabaleshwar, P.N. Vinay Kumar, M. Sheremet, Magneto hydrodynamics flow of a nanofluid driven by a stretching/shrinking sheet with suction, Springer Plus. 5 (2016) 1–19.
[15] M. Sharifpur, A.B. Solomon, T.L. Ottermann, J.P. Mayer, Optimum concentration of nanofluids for heat transfer enhancement under cavity flow natural convection with TiO_2-water, Int. Commun. Heat Mass Transf. 98 (2018) 297–303.
[16] M. Sharifpur, N. Tshimanga, J.P. Mayer. Parametric analysis of effective thermal conductivity models for nanofluids, ASME Int. J. Mech. Eng. Congress Exposition 45257 (2012) 1–11.
[17] L.T. Benos, D.P. Nickolas, U.S. Mahabaleshwar, G. Lorenzini, I.E. Sarris, Thermal and flow investigation of MHD natural convection in a nanofluid-saturated porous enclosure: an asymptotic analysis, J. Therm. Anal. Calorimetry 143 (2021) 751–765.
[18] N. Sandeep, A. Malvandi, Enhanced heat transfer in liquid thin film flow of non-Newtonian nanofluids embedded with graphene nano particles, Adv. Powder Technol. 27 (2016) 2448–2456.
[19] M. Kole, T. Dey, Investigation of thermal conductivity, viscosity, and electrical conductivity of graphene based nanofluids, J. Appl. Phys. 113 (2013), 084307.
[20] N. Ahammed, L.G. Asirvathama, J. Titus, J.R. Bose, S. wongwises, Measurement of thermal conductivity of graphene-water nanofluid at below and above ambient temperatures, Int. Commun. Heat Mass Transf. 70 (2016) 66–74.
[21] E.H. Aly, Dual exact solutions of graphene-water nanofluid flow over stretching/shrinking sheet with suction/injection and heat source/sink: critical values and regions with stability, Powder Tech. 342 (2019) 528–544.
[22] S. Singh, P. Verma, S.K. Ghosh, Numerical and experimental analysis of performance in a compact plate heat exchanger using graphene oxide/water nanofluid, Int. J. Numer. Meth. Heat Fluid Flow 31 (2021) 3356–3372.
[23] U.S. Mahabaleshwar, T. Anusha, P.H. Sakanaka, S. Bhattacharyya, Impact of Lorentz force and Schmidt number on chemically reactive Newtonian fluid flow on a stretchable surface when Stefan blowing and thermal radiation and significant, Arabian Jour. Sci. Eng. (2021) 1–17.
[24] T. Anusha, H.-N. Huang, U.S. Mahabaleshwar, Two dimensional unsteady stagnation point flow of Casson hybrid nanofluid over a permeable flat surface and heat transfer analysis with radiation, J. Taiwan Inst. Chem. Eng. 127 (2021) 79–91.
[25] U.S. Mahabaleshwar, K.N. Sneha, H.uang-Nan-Huang, An effect of MHD and radiation on CNTS-water based nanofluid due to a stretching sheet in a Newtonian fluid, Case Studies Therm. Eng. (2021) 101462.
[26] U.S. Mahabaleshwar, K.R. Nagaraju, P.N. Vinay Kumar, M.N. Azese, Effect of radiation on thermosolutal Marangoni convection in a porous medium with chemical reaction and heat source/sink, Phys. Fluids 32 (11) (2020), 113602.
[27] L.T. Benos, K.R. Nagaraju, U.S. Mahabaleshwar, M.S. Prasad, I.E. Sarris, G. Lorenzini, Magnetohydrodynamic and radiation effects on the heat transfer of a continuously stretching/shrinking sheet with mass transpiration of the horizontal boundary, Chinese Jour. Phys. 72 (2021) 700–715.
[28] K.N. Sneha, U.S. Mahabaleshwar, R. Bennacer, M. EL Ganaoui, Darcy Brinkman equations for hybrid dusty nanofluid flow with heat transfer and mass transpiration, Computation. 9 (2021) 118.
[29] T. Anusha, U.S. Mahabaleshwar, Y. Sheikhnejad, An MHD of nanofluid flow over a porous stretching/shrinking plate with mass transpiration and Brinkman ratio, Trans. Porous medium. (2021) 1–20.
[30] M.M. Bhatti, S.M. Sait, R. Ellahi, Magnetic nanoparticles for drug delivery through tapered stenosed artery with blood based non-Newtonian fluid, Pharmaceuticals 15 (2022) #1352.
[31] R. Ellahi, The effect of MHD and temperature dependent viscosity on the flow of non-Newtonian nanofluid in a pipe: analytical solutions, App. Math. Model. 37 (3) (2013) 1451–1457.
[32] M.M. Bhatti, O.A. Beg, R. Ellahi, M.H. Doranehgard, F. Rabiei, Electro-Magnetohydrodynamics hybrid nanofluid flow with gold and magnetism oxide nanoparticles through vertical parallel plates, J. Magn. Magn. Mater. 564 (2022), 170136.
[33] M. Hassan, A. Zeeshan, A. Majeed, R. Ellahi, Particle shape effects on ferrofluids flow and heat transfer under influence of low oscillating magnetic field, J. Magn. Magn. Mater. 443 (2017) 36–44.
[34] M.F. Ahmed, A. Zaib, F. Ali, O.T. Bafakeeh, E.S.M. Tag-ElDin, K. Guedri, S. Elattar, M.I. Khan, Numerical computation for Gyrotactic microorganisms in MHD radiative Eyring-Powell nanomaterial flow by a static/moving wedge with Darcy-Forchheimer relation, Micromachnes 13 (2020) 1768.
[35] S. Li, M.I. Khan, F. Alzahrani, S.M. Eldin, Heat and mass transport analysis in radiative time dependent flow in the presence of Ohmic heating and chemical reaction, viscous dissipation: an entropy modeling, Case Studies Therm. Eng. 42 (2023), 102722.
[36] O.T. Bafakeeh, K. Raghunath, F. Ali, M. Khalid, E.S.M. Tag-ElDin, M. Oreijah, K. Guedri, N.B. Khedher, M.I. Khan, Hall current and Soret effects on unsteady MHD rotating flow of second-grade fluid through porous media under the influences of thermal radiation, Catalysts 12 (2022). #1233.
[37] S. Li, V. Puneeth, A.M. Saeed, A. Singhal, F.A.M. Al-Yarimi, M.I. Khan, S.M. Eldin. Analysis of the Thomson and troian velocity slip for the flow of ternary nanofluid past a stretching sheet. Sci. Rep, 13, #2340.
[38] M. Shahid, H.M. Asif Javed, M.I. Ahmad, A.A. Qureshi, M.I. Khan, M. A. Alnuwaiser, A. Ahmed, M.Z. Khan, E.S.M. Tag-Eldin, A. Shahid, A. Rafique, A brief assessment on recent developments in efficient electrocatalytic nitrogen reduction with 2-D non-metalic nanomaterials, Nanomaterials 12 (2022) #3413.
[39] H.V. Kirankumar, R. Thejas, C.S. Naveen, M.I. Khan, G.D. Prasanna, S. Reddy, M. Oreijah, K. Guedri, O.T. Bafakeeh, M. Jameel, A review on electrical and gas-sensing properties of reduced graphene oxide-metal oxide nanocomposites, Biomass Conversation Biorefinery (2022) #1105.
[40] A. Abbasi, W. Farooq, E.S.M. Tag-Eldin, S.U. Khan, M.I. Khan, K. Guedri, S. Elattar, M. Waqas, A.M. Galal, Heat transport exploration for hybrid nanoparticle (Cu, Fe2O4)-based blood flow via tapered complex wavy curved channel with slip features, Micromachines 13 (2022). #1415.
[41] H. Waqas, M. Oreijah, K. Guedri, S.U. Khan, S. Yang, S. Yasmin, M.I. Khan, O. T. Bafakeeh, E.S.M. Tag-Eldin, A.M. Galal, Gyrotactic Motile microorganisms impact on Pseudoplastic nanofluid flow over a moving riga surface with exponential heat flux, Crystals 12 (2022). #1308.